The Cryosphere
Open Access
EGU
Discussions

Ground-penetrating radar imaging reveals glacier's drainage network in 3D

Gregory Church[1,2], Andreas Bauder[1], Melchior Grab[1,2], and Hansruedi Maurer[2]

[1]Laboratory of Hydraulics, Hydrology and Glaciology (VAW), ETH Zurich, Zurich, Switzerland
[2]Institute of Geophysics, ETH Zurich, Zurich, Switzerland

Correspondence: Gregory Church (church@vaw.baug.ethz.ch)

Abstract.

Hydrological systems of glaciers have a direct impact on the glacier dynamics. Since the 1950's, geophysical studies have provided insights into these hydrological systems. Unfortunately, such studies were predominantly conducted using 2D acquisitions along a few profiles, thus failing to provide spatially unaliased 3D images of englacial and subglacial water pathways. The latter has likely resulted in flawed constraints for the hydrological modelling of glacier drainage networks. Here, we present for the first time 3D ground-penetrating radar (GPR) results that provide unprecedented high-resolution 3D images of an alpine glacier's drainage network. Our results confirms a long-standing englacial hydrology theory stating that englacial conduits flow around glacial overdeepenings rather than directly over the overdeepening. Furthermore, these results also show exciting new opportunities for high-resolution 3D GPR studies of glaciers.

1 Introduction

Glacier movement is the combination of internal ice deformation and basal motion. Basal motion comprises both ice sliding over the glacier bed and the deformation of subglacial till (Cuffey and Paterson, 2010). Sliding at the ice-bed interface is responsible for high ice flow velocities (often 100%-400% faster than the annual mean flow velocity (Macgregor et al., 2005; Bingham et al., 2006; Bartholomew et al., 2010; Tuckett et al., 2019)) as a result of reduced friction at the ice-bed interface (Bartholomaus et al., 2008). This reduction of friction is caused by the subglacial drainage network that lubricates this interface and increases subglacial water pressure, thereby either weakening subglacial sediments (Schoof, 2010) or lubricating the hard bedrock. In alpine glaciers and in Greenland, the subglacial drainage network is fed from surface meltwater that is routed through the englacial drainage network (Fountain and Walder, 1998). At the beginning of the melt season and with an increased availability of surface melt water, the subglacial drainage network often experiences an increase in water pressure, since the drainage network cannot adapt quickly enough to the increase in meltwater influx (Iken et al., 1983). During these periods with increased subglacial water pressure, changes in the glacier's sliding velocity are often observed (Gudmundsson et al., 2000; Sugiyama and Gudmundsson, 2004; Macgregor et al., 2005), and it has been widely documented that increased glacier sliding velocities have the potential to increase the glacier's mass loss (Zwally et al., 2002; Joughin et al., 2008; Schoof, 2010). Whilst the existence of these variations in ice flow velocities are undisputed, there is limited observations of the hydrological system's

The Cryosphere
Discussions

25 geometry and its temporal variations, thus hampering a deeper understanding of these seasonal variations (Hart et al., 2015;
Church et al., 2020).

The glacier's hydrological system can be probed using a variety of methods. Direct observations have been made from
boreholes (Fountain et al., 2005), tracer testing (Nienow et al., 1996), speleology (Gulley, 2009; Gulley et al., 2009; Tem-
minghoff et al., 2019) and geophysical measurements. The latter include predominantly active (Peters et al., 2008; Zechmann
30 et al., 2018; Church et al., 2019) and passive (Podolskiy and Walter, 2016; Lindner et al., 2019; Nanni et al., 2020) seismic
measurements or ground-penetrating radar (GPR) measurements (Moorman and Michel, 2000; Stuart et al., 2003; Irvine-Fynn
et al., 2006; Harper et al., 2010; Bælum and Benn, 2011; Hansen et al., 2020). Most GPR studies, published so far, relied on
two-dimensional (2D) data, where GPR measurements were acquired along profiles. 2D data sets are typically unable to image
complex subsurface structures, such as glacier drainage networks, and the resulting interpretations may thus be inconclusive.
35 For small-scale targets, such as archaeology sites (Böniger and Tronicke, 2010) and shallow fault zones (McClymont et al.,
2008), 3D GPR surveys have established themselves as a powerful and efficient option to image complex subsurface structures.
However, spatially unaliased 3D GPR data sets (i.e., datasets with a data point spacing smaller than the dominant wavelength
of the GPR signals (Sheriff and Geldart, 1995; Grasmueck et al., 2005)) are uncommon in glaciological applications. This
is unfortunate, because 3D GPR provides subsurface images that can be viewed from arbitrary directions, thus allowing for
40 an unequivocal interpretation. Such an approach would be particularly useful for glacier drainage networks, and should be
feasible because of the strong reflections caused by the very pronounced electrical impedance contrasts at ice/water interfaces
(Reynolds, 1997).

In this study we demonstrate the feasibility of and opportunities offered by 3D GPR imaging on glaciers. Therefore, we
performed a 3D GPR survey over a temperate alpine glacier to delineate the drainage network and provide much needed
45 hydrological observations to confirm long-standing glacier hydraulic theory. Furthermore, such GPR surveys are able to provide
an insight into future opportunities for high-resolution radar studies of glaciers.

2 Survey Site

The 3D GPR acquisition was conducted on Rhonegletscher, a temperate glacier located in the central Swiss Alps (Fig. 1a).
It is representative for the majority of European mountain glaciers with regard to its temperature distribution, ice dynamics
50 and size (GLAMOS, 2017; Beniston et al., 2018). Rhonegletscher is the sixth largest glacier in the Swiss Alps (length: 8 km,
surface area: 15.5 km^2 as of 2015 (GLAMOS, 2017)) and is heavily exposed to glacier melt due to the changing climate. Over
the last decades, the glacier has continued to thin and it is currently retreating. As a result, a proglacial lake fed by the drainage
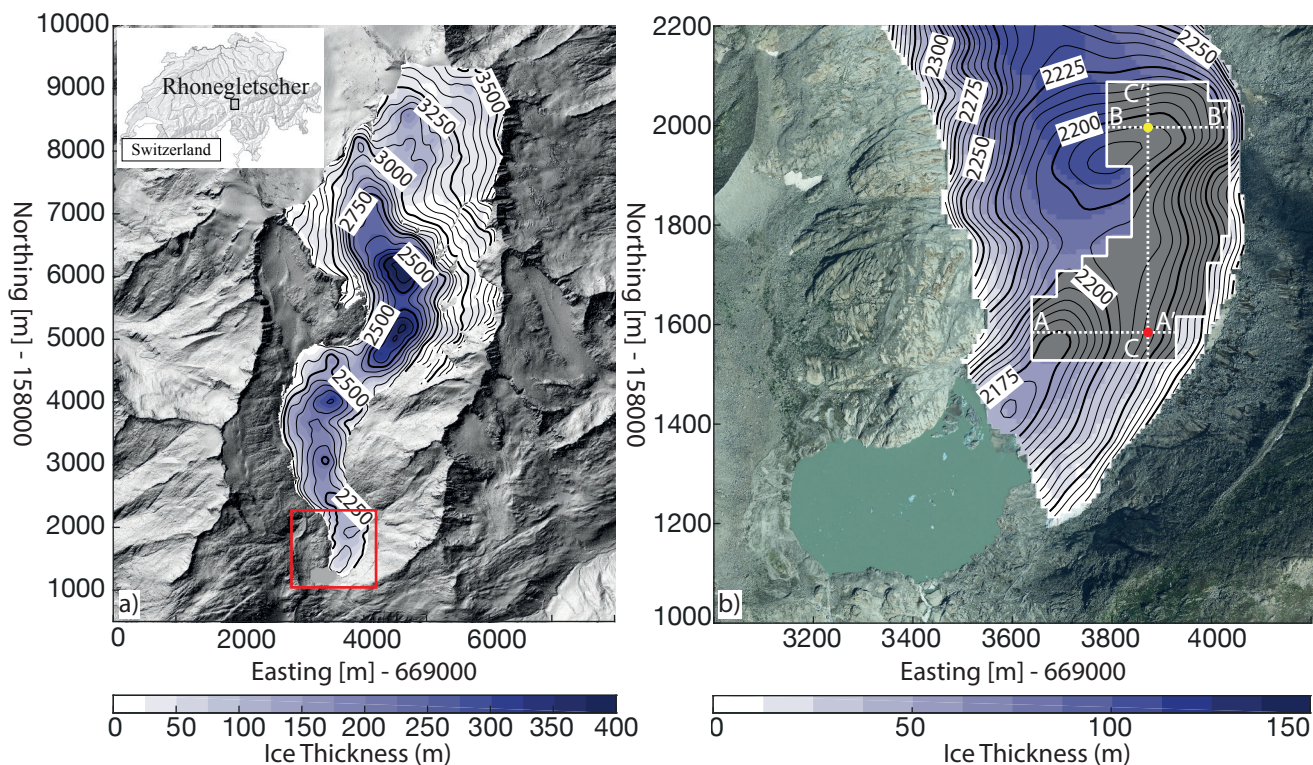network has been forming at its terminus since 2005 (Tsutaki et al., 2013).

Figure 1. a) Rhonegletscher ice thickness in 2019 (colours) and bedrock elevation (contours) estimated using GlaTe modelling 59 from interpolated radar profiles. The red box represents the zoomed area for panel (b). b) Lower ablation zone of Rhonegletscher showing ice thickness (colour) and bedrock elevation (contours). The grey polygon represents the 3D GPR survey site, three GPR profiles A-A', B-B' and C-C' are shown in Figure 2 and the crossing points of the GPR profiles are represented by a yellow and red dot. Co-ordinates for all plots are local swiss co-ordinates LV03. Orthophoto was provided by Swiss Federal Office of Topology: Reproduced by permission of swisstopo (JA100120), ©2020 swisstopo (JD100042)

3 Methods

3.1 Data Acquisition

55

To detect and characterise the drainage network located at the glacier's tongue, we acquired a high-resolution 25 MHz 3D GPR survey. This survey was motivated by the results of earlier 2D surveys including active seismic data (Church et al., 2019), repeated GPR measurements on a coarse grid of 2D lines (Church et al., 2020) and a drilling campaign in 2018, which provided initial imaging of a potential drainage network. Between 15th July 2020 and 23rd July 2020, GPR data were acquired over the

60 area expected to harbour the englacial conduit network (Fig. 1b).

The survey covered an area of 140,000 m^2, within which the ice thickness varied between 25 and 110 m and where the glacier bed forms a distinct overdeepening (Fig. 1b). The common-offset GPR data were collected using a Sensor & Software

PulseEkko® system with an antenna separation of 4 m and carried by hand at approximately 1 m above the glacier ice surface. The sampling rate of the GPR system was 1 GHz, giving a time resolution of 1 ns, and thereby providing a vertical spatial

65 resolution in temperate ice of 0.168 m. The use of a large sampling frequency allows small topographical changes from trace to trace of <0.2 m to be observed (King, 2020). A GPR stacking of 4 improved the signal-to-noise ratio and allowed the GPR data to be acquired with average walking speed of approximately 0.4 m per GPR trace. For all GPR lines, a high precision global navigation satellite system (GNSS) continuously recorded the x, y, z coordinates of the centre point between the transmitting and receiving antennas every second. The average accuracy of the GNSS during GPR acquisition was 0.008 m.

70 The survey area was covered with 281 profiles, resulting in a total profile length of approximately 85 km. The 3D GPR data were collected perpendicular to the ice flow direction and profiles were interspaced 2 m. The line spacing was chosen, such that the diffractions and reflections within the ice body would not become aliased for our antenna frequency of 25 MHz. To ensure data were consistent across the duration of the survey, two GPR lines were always repeated from the previous day's acquisition. Furthermore, six orthogonal profiles were collected along the glacier flow.

75 ### 3.1.1 Data Processing

All GPR common offset data were processed using a combination of an in-house MATLAB-based toolbox (GPRglaz) (Grab et al., 2018) and SeisSpace ProMAX 3-D. The processing was based upon a typical 3D seismic data processing workflow. Initially, the GPR data were assigned to their corresponding GNSS data. Since the GNSS data were recorded every second and GPR data were recorded approximately every 0.3 seconds, the GNSS data were linearly interpolated to provide the same

80 temporal resolution as the GPR data. The data were then corrected for time zero, and a Butterworth bandpass filter was applied in order to suppress any noise outside the GPR frequency band and thus to increase the signal-to-noise ratio. Overlapping GPR data between different acquisition days were used to investigate whether a data matching filter was required. However, no amplitude matching was required, due to the fact that the GPR equipment used produced stable and repeatable GPR data. Subsequently, the data were 3D binned using a master grid of 2 m between GPR profiles (inline spacing) and 0.5 m between

85 GPR data points within the profile (crossline spacing). 3D binning consists of assigning each GPR trace to the closest bin centre. As a result of the variable walking speed and walking around crevasses during acquisition, a number of bins had more than a single GPR trace assigned (known as over-fold), whereas other bins (i.e. bin located within a crevasse) were empty. GPR data points were removed from bins that had more than one GPR data point and therefore, this resulted in the bins containing either a single GPR data point or no GPR data point. Such a processing step is required in order not to leave an amplitude

90 imprint on the data during the interpolation and regularisation stages. The data were interpolated and regularised, such that each bin within the survey boundary had an interpolated GPR trace at the centre of the bin.

A 3D Kirchhoff migration algorithm re-positioned the reflected and diffracted signals back to their correct subsurface location. The Kirchhoff migration algorithm was performed using EM wave propagation velocity of ice (0.167 m ns^{-1}) and furthermore, the algorithm corrected for amplitude losses from geometrical spreading. Prior to interpretation the data were

95 corrected for attenuation using a Q compensation (Irving and Knight, 2003), a second Butterworth bandpass filter was applied

to further improve the signal-to-noise ratio, and the data were stretched from the time to depth domain using a constant velocity of 0.167 m ns^{-1}.

The 3D interpretation was performed in dGB Earth Sciences OpendTect. The ice-bed interface was manually picked, linearly interpolated, smoothed and constrained to within the survey area. Similarly, the drainage network was picked at a similar horizontal spacing, linearly interpolated and smoothed. The spatial extent of the drainage network was determined from the GPR depth slices (Fig. 3) and also by extracting the root-mean squared amplitude between the surface and the ice-bed interface. Finally, the reflected GPR amplitudes were extracted from both the ice-bed interface and the drainage network by using a 2 m window ($\pm$1 m) centred around the feature.

4   Results

4.1   Overview of GPR results

Displaying 3D models adequately is generally a non-trivial task. Below, we discuss the GPR results using a variety of vertical and horizontal cross sections. In our view, such data sets are represented best in form of movies showing scans along different directions. We therefore highly encourage the readers to check the digital supplement.

Selected 2D profiles of the 3D GPR data cube are shown in Figure 2. A water-filled englacial conduit can be identified as a continuous specular strong reflector (Fig. 2a, b, c). The ice-bed interface is identifiable as a weak reflection (Fig 2), indicating that subglacial water is not present. However, in isolated areas, the ice-bed interface has been identified as strong ice-bed reflections (Fig. 2c) and thereby indicating the presence of subglacial water.

The lateral extent of the englacial and subglacial network can be characterised by analysing horizontal slices of the 3D GPR data cube. A slice at 2216 m.a.s.l shows a strong meandering reflection in the northern part of the survey (Fig 3a). The strong reflection is traceable on the eastern edge of the survey before fading out towards the southern edge. At 2213 m.a.s.l (Fig 3b), there is a continuation of the strong reflection, but it becomes more diffusive in the central part of the survey area. At 2210 m.a.s.l (Fig. 3c), we observe another strong meandering reflection that heads southwards towards the terminus of the glacier. There is an approximately 6 m topographic difference between the drainage network in the survey's northern edge and the southern edge indicating that the imaged drainage network has a shallow global inclination along the flow (<1 degree).

4.2   Spatial distribution of drainage network

The 3D GPR survey imaged an active meltwater drainage network within the survey boundary. It comprises both, an englacial and subglacial drainage network. The entire drainage network was identified from the GPR data, and reflected amplitudes from the drainage network were extracted (Fig 4a). The conduit network can be delineated by areas of high amplitude (red in Fig. 4a). Furthermore, the drainage network can be split into four separate components labelled in Fig. 4b:

(A) A meandering well-defined englacial conduit spanning the overdeepen oriented perpendicular to the glacier flow,
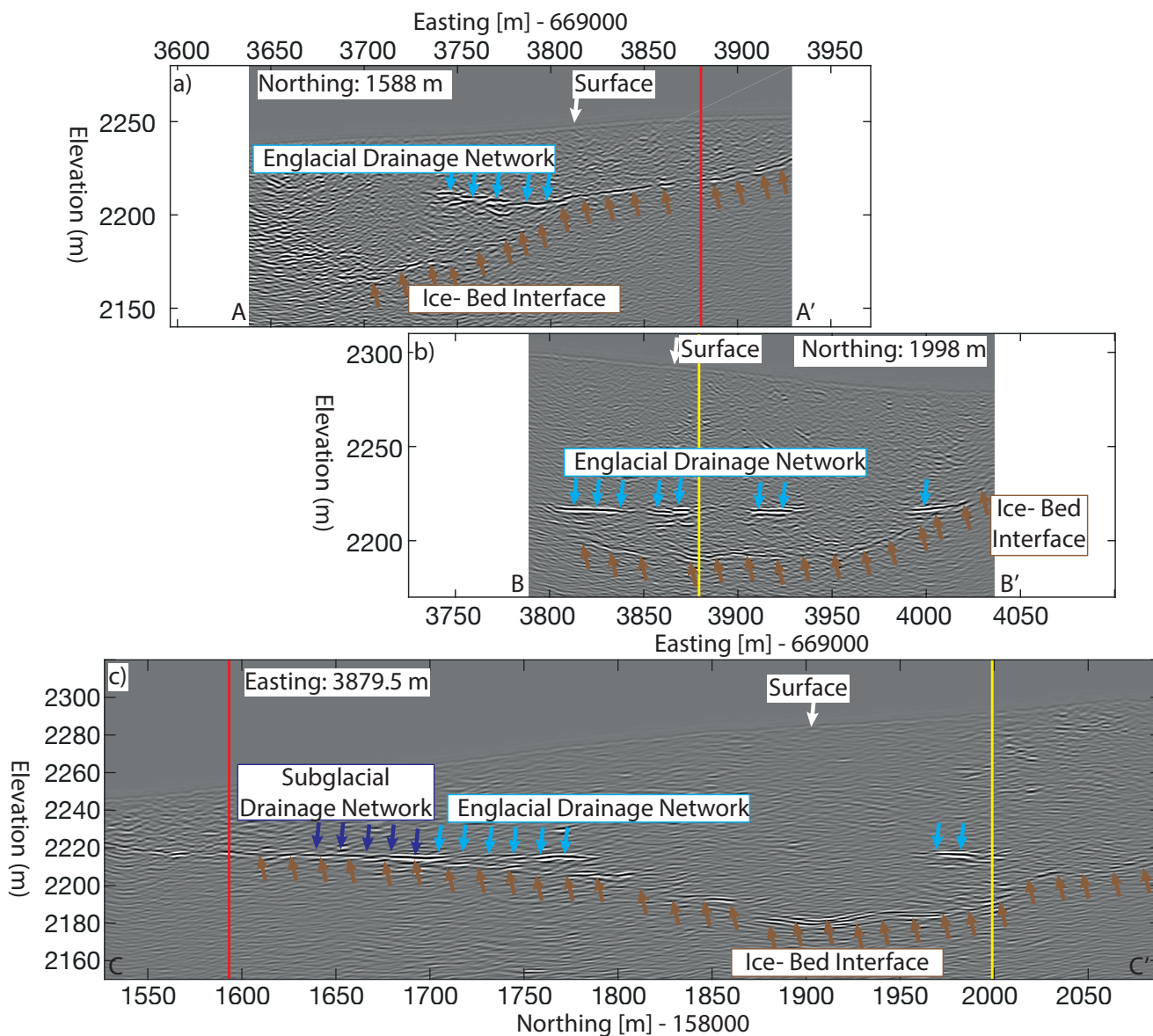
Figure 2. a) GPR inline profile (perpendicular to ice-flow direction), the glacier surface, drainage network and basal interface are marked and the red line represents the crossing point for profile c). b) GPR inline profile (perpendicular to ice-flow direction), the yellow line represents the crossing point for profile c). c) GPR crossline profile (parallel to ice-flow direction). The locations of the profiles are shown in Figure 1b and 3

(B) An englacial conduit oriented parallel to the glacier flow traversing the overdeepen and flowing alongside the glacier's flank,
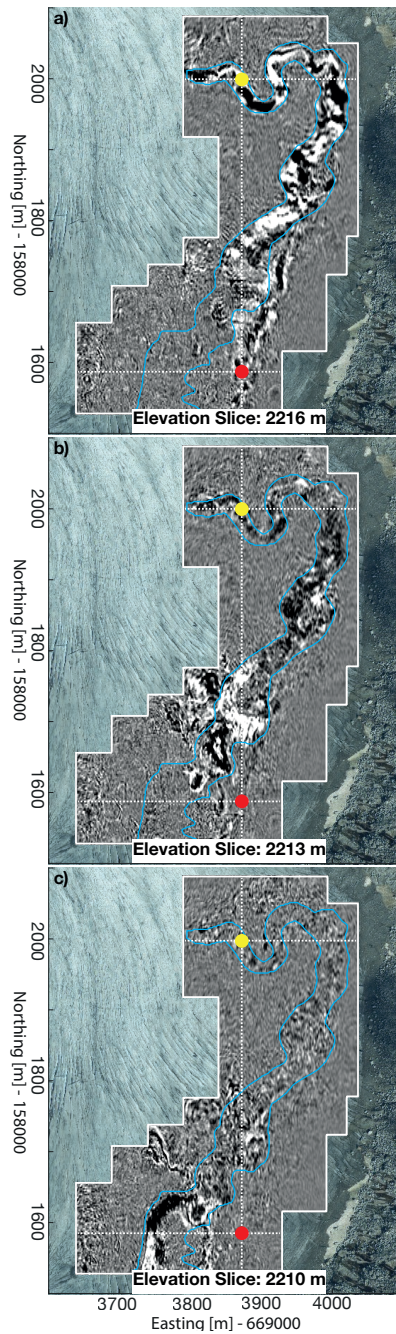
Figure 3. a) Depth slice through the GPR 3D data cube at 2216 m amsl. b) 2213 m amsl. c) 2210 m amsl. The blue line represents the outline of the drainage network. The white dashed line represents the GPR profiles from Figure 2 and the red and yellow dot represents their crossing points.
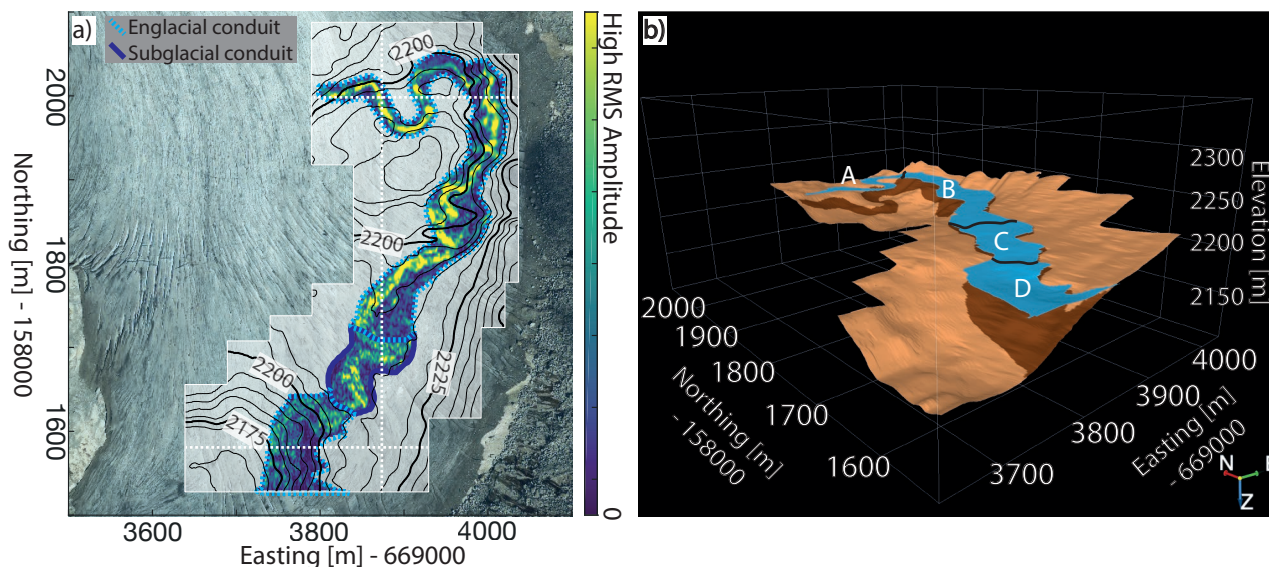
Figure 4. a) The root-mean-squared amplitude, extracted from the picked glacial drainage network, within ±1 m of the drainage network. Contours represent the basal topography. Colours of the drainage network represent the reflected amplitudes and areas of high amplitude indicate the presence of water. b) 3D view of basal interface (brown) and drainage network (blue). The drainage network is split into 4 components labelled A to D and referred to in the text.

(C) The englacial conduit in B flows into a subglacial drainage system, the subglacial drainage network consists of a single main conduit (Fig 4a), that has a sinusoidal nature,

130 (D) The subglacial conduit in C encounters a basin and flows into another englacial conduit towards the terminus of the glacier.

Given the glacier ice flow direction (N-S) and the ice-thickness distribution, the conduit is expected to flow from north to south. The high-resolution results allow the width of the drainage network to be examined. The mean width of the northern si-nusoidal englacial conduit, which flows across the overdeepening (Fig. 4b Section A), is 8 m. As the network flows southwards 135 around the overdeepening (Fig. 4b Section B) the width increases to 11 m. Furthermore, the mean width of the subglacial drainage conduit (Fig. 4b Section C) is 17 m, and finally at the southern edge of the survey site, the mean width of the englacial drainage network is 25 m (Fig. 4b Section D). The thickness of the conduit in section A has previously been investigated in Church et al. (2020), and it was found to be at the limit of the 25 MHz GPR vertical resolution at 0.4 m, when assuming the conduit is water-filled. The conduit thickness in sections B, C and D are also at the limit of the vertical resolution as only a 140 single reflection is visible (Fig. 2c). If the conduit thickness was beyond the vertical resolution, two separate englacial reflec-tions would be visible representing the top and bottom of the conduit. Consequently, the channels throughout the study area are thinner than 0.4 m, and therefore, their shape is significantly smaller in the vertical direction than lateral.

4.3 Basal reflected amplitude

The amplitude of the ice-bed interface was extracted from the basal horizon as well. This provided insights into the local
145 basal conditions. In the southern region of the survey site, the ice-bed interface reflection has identical amplitude and spatial distribution to the drainage network (Fig. 5a and c white arrows), thereby indicating this area is positioned along the main drainage network identified in Figure 4. In the northern region of the survey site, instead, there are numerous isolated high amplitudes basal reflections (Fig. 5a), mostly situated within localised flat areas (Fig. 5 b red arrows) indicating a pooling of water. In addition, ubiquitous areas of high amplitude basal reflections are present along the southern region of the survey,
150 indicating the presence of subglacial water (Fig. 5a and c pink arrows). In comparison to the isolated patches in the northern region, these high amplitude basal patches in the southern region appear to be connected to each other indicating the possibility of an additional connected subglacial drainage system.

4.4 Comparison of 2D and 3D GPR processing

2D GPR surveys along single profiles are the current approach in today's glaciological applications, although such data sets
155 have imaging limitations. Besides being unable to provide 3D subsurface images, 2D GPR techniques assume all reflections originate from the vertical plane of the acquisition. Complex englacial structure or basal geometry can result in a reflection originating from outside of the acquisition plane, in turn resulting in distortions to the final processed GPR image. Figure 6 shows an example of such a distortion. These distortions are particularly severe for complex geometry of alpine glaciers

3D GPR acquisition and processing are able to mitigate these distortions. The Rhonegletscher GPR data cube is the product
160 of a 3D processing workflow and with the employment of 3D migration over conventional 2D migration, the distortions from out-of-plane reflections are removed and an improvement in lateral resolution is gained. A 3D migration effectively collapses the Fresnel zone in both inline and crossline directions, thereby reducing the lateral resolution to the 3D bin size (2 m x 0.5 m). This lateral resolution improved leads to improvements in subsurface imaging, as two closely laterally-separated reflectors are able to be imaged as two individual reflectors.

165 A comparison between GPR data processed with two different workflows (2D GPR workflow (Figure 7a) and 3D GPR workflow (Fig. 7b)) highlights the imaging differences on both the englacial conduit network and the ice-bed interface. Generally, both workflows produce similar subsurface images however, there are subtle differences that indicate a more unambiguous interpretation with the 3D GPR workflow. The ice-bed interface in the 3D GPR data cube has increased reflector continuity in comparison to the 2D workflow (Fig. 7 brown arrows). Furthermore, the englacial conduit imaged using a 3D GPR workflow
170 has fewer artefacts and is absent of events that are incorrectly intersecting the englacial conduits (Fig. 7 blue arrows).
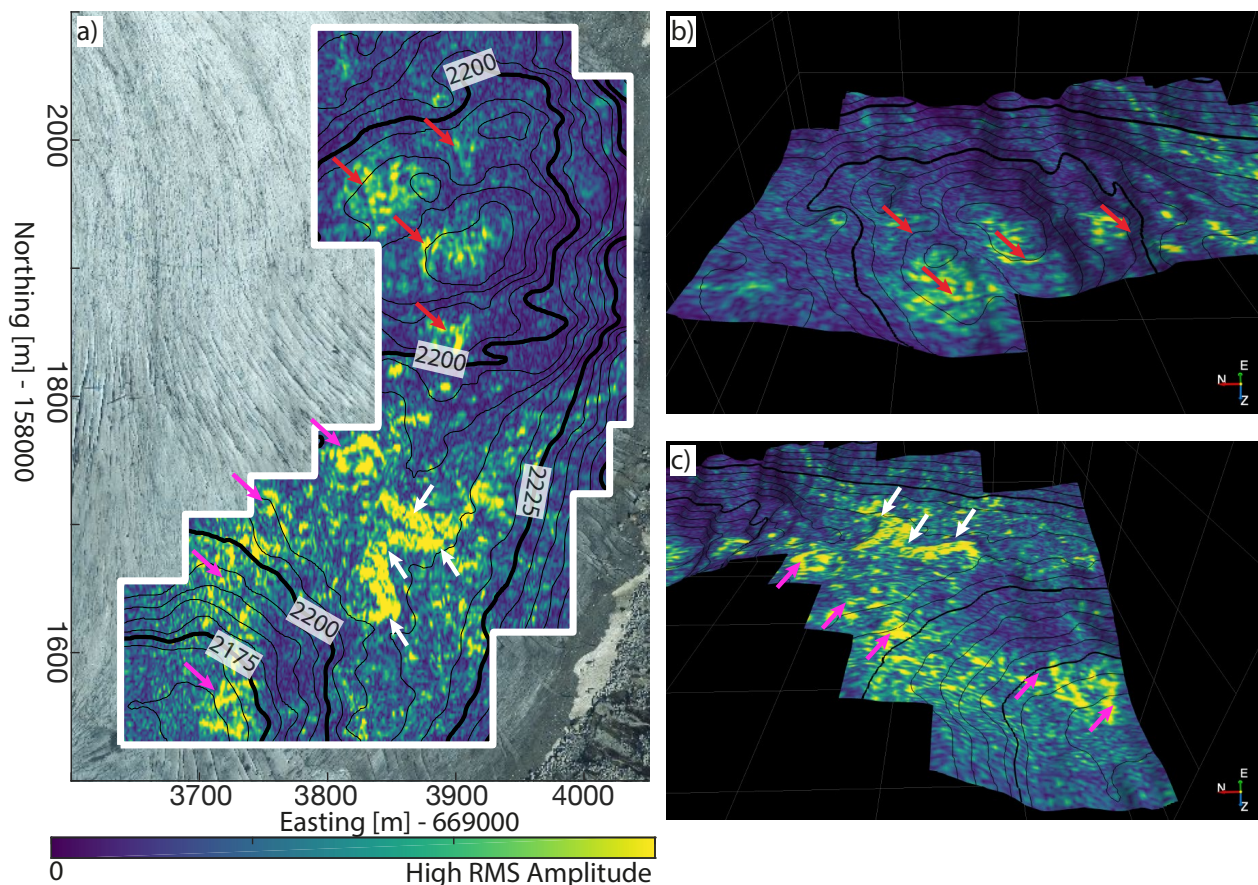
Figure 5. a) Map view of the extracted basal root-mean squared amplitude within a ± 1 m window. Contours represent the basal topography. b) Extracted basal amplitude in the northern part of the survey highlighting isolated high amplitude basal reflections situated in localised flat zones, c) extracted basal amplitude in the southern part of the survey highlighting connected high amplitude basal reflections. The red arrows represent isolated water cavities along basal interface, the white arrows represent the main drainage network detected in Fig. 4. The pink arrows indicate the presence of subglacial water flow away from the main drainage network identified in Fig 4.

5 Discussion

5.1 Geometry of drainage network

This is the first time that a glacier's drainage network is imaged in 3D with GPR data, thus providing an unprecedented, high-resolution information of the geometry from such a system. In our case, it has a meandering nature throughout the survey area, and the drainage network's width increases towards the terminus of the glacier. Moreover, it consists of a single dominant conduit that alternately flows englacial and subglacial. Such a drainage network is known as an efficient channelised network. Studies from both cold-ice (Chandler et al., 2013) and temperate-ice (Nienow et al., 1996, 1998; Mair et al., 2002) glaciers
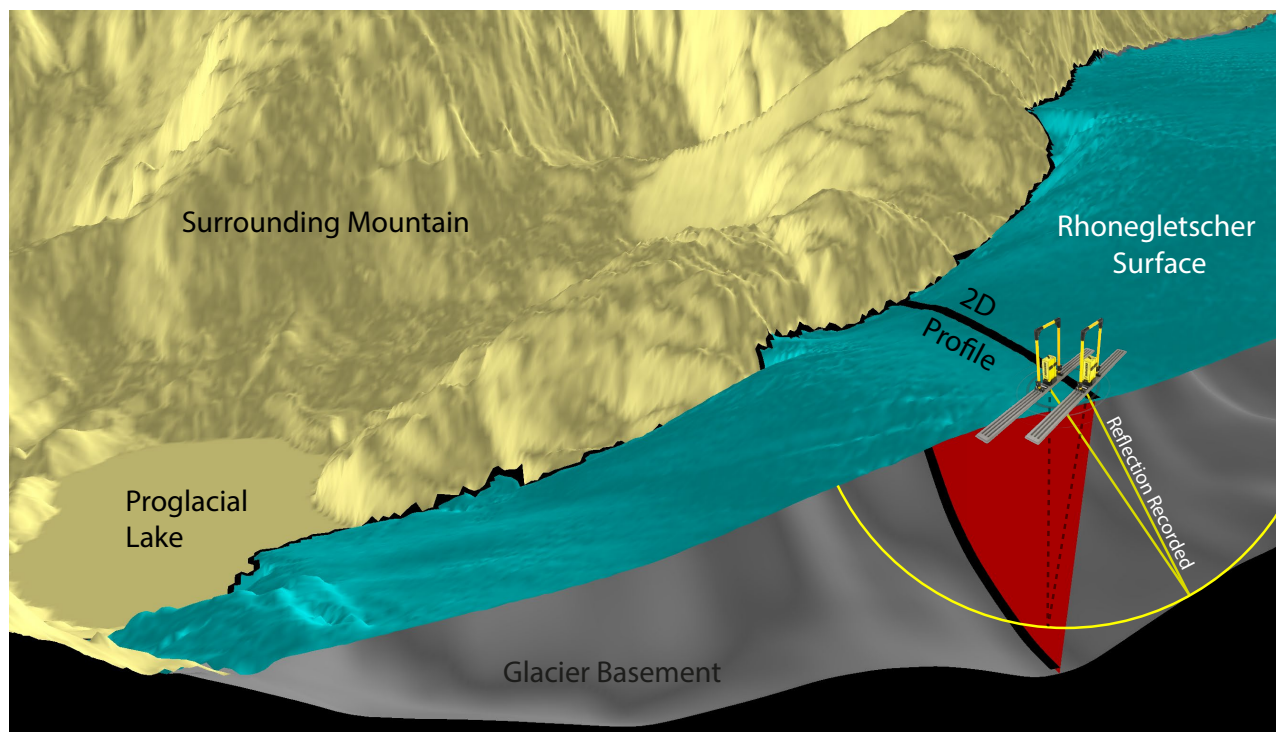
Figure 6. Lower portion of Rhonegletscher showing an example GPR data point acquired. The GPR antennas are located on the surface and the yellow lines represent the shortest ray path for a reflection from the glacier basement. The dashed black ray path represents the basement imaging point when performing 2D GPR processing. This ray path does not correspond to the true basement position but the out-of-plane basement reflection point.

have shown that early in the melt season, the glacier's drainage network is slow and inefficient. Typically, it evolves into a fast channelised drainage network just before the peak of the glacier's discharge. Since the peak discharge for Rhonegletscher is

180   typically mid-August (GLAMOS, 2017) and thus occurred one month after the acquisition, the drainage network is expected to be in a channelised configuration. The 3D GPR imaging results confirm that the network consists of a single, wide conduit, that alternately flows through englacial and subglacial channels, known as Röthlisberger channels (Röthlisberger, 1972).

The theoretical shape of englacial drainage conduits is circular, however the drainage network imaged on Rhonegletscher is up to a maximum of 60 times wider than its thickness. Such an observation contradicts the theory of circular conduit cross-

185   sectional shape proposed independently by Shreve and Röthlisberger (Röthlisberger, 1972; Shreve, 1972) but is in line with the further development by Hooke et al. (1990).

Lliboutry (1983) hypothesised that when water encounters an overdeepening, the water flows along the glacier's flank as so-called gradient conduits, therefore avoiding the deepest part of the overdeepening (Cook and Swift, 2012). According to Lliboutry's theory, these conduits should be located at the same altitude as the lowest point of the riegel that produces the

190   overdeepening. The 3D GPR data suggest that in the case of Rhonegletscher, the flow paths indeed route meltwater around the
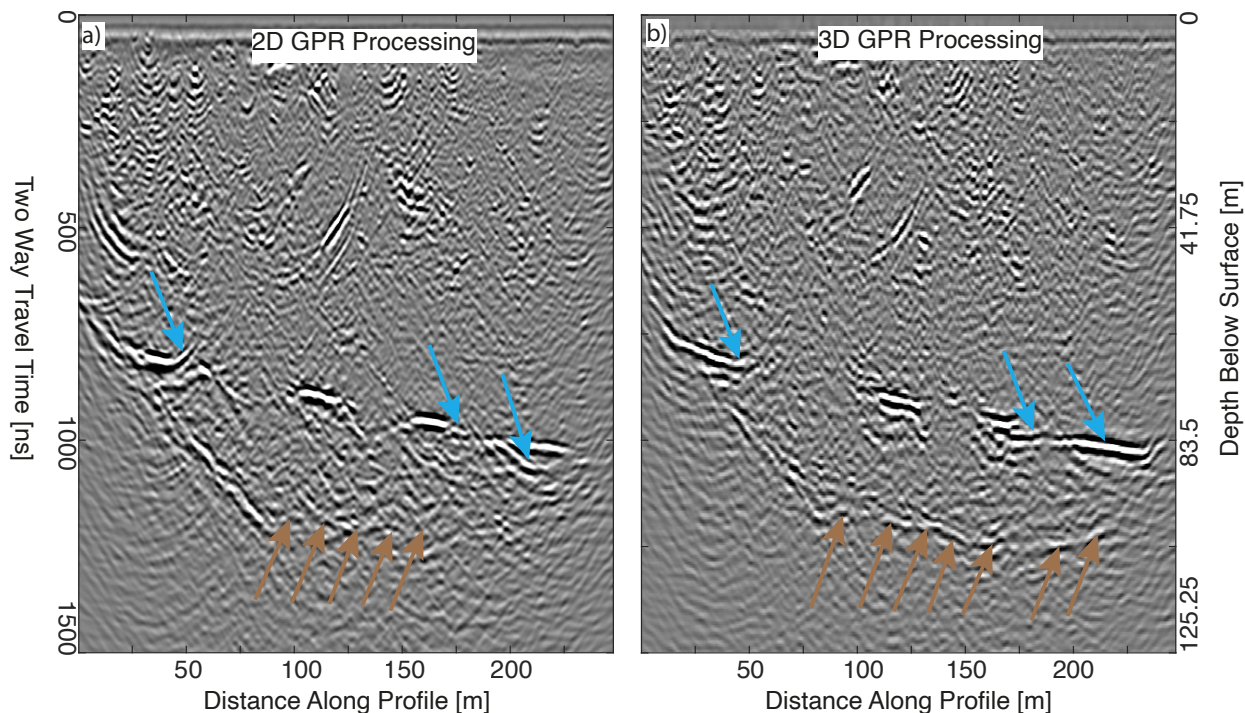
Figure 7. a) A single GPR data profile processed using with a 2D GPR workflow. b) Single line extracted from multiple GPR profiles processed using a 3D GPR workflow.

overdeepening rather than across it (Fig. 4b Labelled: B). Similarly, the elevation of the englacial conduit that is located around the overdeepening coincides with the elevation of the riegel and also the proglacial lake level. These observations support the long-standing theory, but was never verified by field observations.

Subglacial and englacial water flows as a response of changing hydraulic potentials. This hydraulic potential can be es-
195 timated by assuming spatially uniform flotation fraction as described in Flowers and Clarke (1999) and within the imaged Rhonegletscher's drainage network the water flow routing followed the gradient of the hydraulic potential and not along a single hydraulic potential contour.

5.2 Water accumulation in temperate glaciers

In addition to the detection of the primary drainage network, the 3D GPR data provided evidence of subglacial water accumu-
200 lation. GPR-based detection of large amounts of subglacial water, such as subglacial lakes is well established (Ridley et al., 1993; Siegert et al., 2005; Palmer et al., 2013), but their spatial extent is often unclear as a result of the limitations of 2D GPR surveys. This is in contrast to our 3D GPR data set, which can be used to delineate such extents. In addition, 3D GPR has the potential to identify smaller subglacial water accumulations, such as expected to occur within water-filled cavities. Subglacial cavities can form, when the sliding ice uncouples from the glacier bed as a result of either rapid glacier sliding or pronounced

205 bed roughness (Nye, 1970). Two types of subglacial cavity system are generally distinguished – isolated cavities and linked cavities – and both cavity systems alter the glacier's dynamics (Lliboutry, 1976, 1979; Hoffman et al., 2016; Rada and Schoof, 2018). The high amplitude reflections along the basal interface (Fig 5a) represent water accumulations and appear to be isolated from each other, thereby indicating that they are potentially isolated water-filled cavities forming an inefficient drainage network. It is interesting to note both an inefficient drainage network and an efficient network can coexist in overdeepenings

210 (Hooke et al., 1990; Rada and Schoof, 2018). Although our data provide an instantaneous image of these systems, repeated 3D GPR surveys could also yield insights into their temporal dynamics.

5.3 Future of 3D GPR within glaciology

A 3D approach as presented within this contribution is feasible and highly beneficial over 2D GPR for detecting and quantifying dimension of a glacier's hydrological network. For large-scale investigations in Greenland and Antarctica, it will be more

215 challenging to conduct 3D GPR surveys as a result of their spatial distribution and therefore, 2D GPR acquisition will likely continue to prevail. However, future radar surveys could be complimented with the use of 3D GPR acquisition, in order to reduce the ambiguity of interpretations in places of interest.

The major limiting factors of such future 3D GPR surveys are the rate of acquisition and the accessibility of the field site. Both of these concerns can be addressed with drone technology. Drone technology is often used in cryosphere research (Gaffey

220 and Bhardwaj, 2020) however GPR-based drone surveys are currently limited to landmine detection (Colorado et al., 2017; Sipos et al., 2017) and soil mapping (Wu et al., 2019). Developments of lightweight GPR systems are anticipated to provide the possibility of equipping small, uncrewed aerial vehicles (UAVs) with the capabilities to acquire 3D radar data in a fast and efficient manner. With sufficient power a drone-based solution would acquire the Rhonegletscher data within an estimated 7 hours of flying time, instead of 9 days spent for the ground-based study.

225 6 Conclusions

By using a 3D GPR data set, we have produced unaliased imaging of the Rhonegletscher's drainage network in a section of its ablation zone that has led to confirming long-standing glacier hydraulic theory. Upon meeting an overdeepening, melt water is routed alongside the flank of the glacier within so-called gradient conduits and thereby avoiding the overdeepening.

The geometry of the drainage network was determined by extracting the root-mean-squared reflected GPR amplitude. Using

230 this extracted GPR attribute, we were able to delineate a hydrological system in 3D, which includes connected englacial and subglacial conduits. Such observations were only possible due to the 3D nature of our data. 2D GPR imaging would have failed in determining the interconnectability of this hydraulic system and with such 2D GPR data a connection would only be the result of speculation. We found the dimensions of the conduit were 60 times wider than its thickness, which is in contrast to theory. However, these observations are in line with further conduit geometry developments by Hooke et al. (1990). From the

235 geometry of the conduit network, we are able to confirm that the hydraulic system is an as efficient drainage network.

In addition to observing the main efficient drainage network, the extracted GPR reflected amplitude from the glacier's basal interface indicated that subglacial water is potentially pooling in numerous isolated localised flat areas. This localised pooling of water forms an inefficient drainage network. Thereby, both an efficient and inefficient drainage networks are able to coexist within overdeepenings.

240   3D GPR data have been adopted and have proven to be successful for imaging small-scale targets within the fields of archaeology and investigating shallow fault zones. This study illustrates the feasibility and the opportunities that are offered by implementing 3D GPR to image glaciers and their hydraulic networks. Alongside the development of lightweight GPR systems and uncrewed aerial vehicles, such future 3D GPR surveys will be acquired faster and in a more efficient manner and thereby ultimately lead to significant improvements in our understanding of glacier hydrology.

245   *Video supplement.* Movies showing inline, cross and depth slices through the 3D GPR cube can be found at https://doi.org/10.3929/ethz-b-000471304

Author contributions. GC, MG, AB, and HM designed the 3D GPR experiment, which were carried out by GC. GC processed the data and interpreted the data, with help from all co-authors. GC wrote the manuscript with comments and suggestions for improvements from all co-authors.

250   *Competing interests.* The authors declare that they have no conflict of interest.

References

260 Bælum, K. and Benn, D. I.: Thermal structure and drainage system of a small valley glacier (Tellbreen, Svalbard), investigated by ground penetrating radar, The Cryosphere, 5, 139–149, https://doi.org/10.5194/tc-5-139-2011, 2011.

Bartholomaus, T. C., Anderson, R. S., and Anderson, S. P.: Response of glacier basal motion to transient water storage, Nature Geoscience, 1, 33–37, https://doi.org/10.1038/ngeo.2007.52, 2008.

Bartholomew, I, Nienow, P., Mair, D., Hubbard, A., King, M. A., and Sole, A.: Seasonal evolution of subglacial drainage and acceleration
265 in a Greenland outlet glacier, Nature Geoscience, 3, 408–411, https://doi.org/10.1038/ngeo863, 2010.

Beniston, M., Farinotti, D., Stoffel, M., Andreassen, L. M., Coppola, E., Eckert, N., Fantini, A., Giacona, F., Hauck, C., Huss, M., Huwald, H., Lehning, M., López-Moreno, J. I., Magnusson, J., Marty, C., Morán-Tejéda, E., Morin, S., Naaim, M., Provenzale, A., Rabatel, A., Six, D., Stötter, J., Strasser, U., Terzago, S., and Vincent, C.: The European mountain cryosphere: A review of its current state, trends, and future challenges, Cryosphere, 12, 759–794, https://doi.org/10.5194/tc-12-759-2018, 2018.

270 Bingham, R. G., Nienow, P. W., Sharp, M. J., and Copland, L.: Hydrology and dynamics of a polythermal (mostly cold) High Arctic glacier, Earth Surface Processes and Landforms, 31, 1463–1479, https://doi.org/10.1002/esp.1374, 2006.

Böniger, U. and Tronicke, J.: Improving the interpretability of 3D GPR data using target-specific attributes: application to tomb detection, Journal of Archaeological Science, 37, 360–367, https://doi.org/10.1016/j.jas.2009.09.049, 2010.

Chandler, D. M., Wadham, J. L., Lis, G. P., Cowton, T., Sole, A., Bartholomew, I., Telling, J., Nienow, P., Bagshaw, E. B., Mair, D., Vinen,
275 S., and Hubbard, A.: Evolution of the subglacial drainage system beneath the Greenland Ice Sheet revealed by tracers, Nature Geoscience, 6, 195–198, https://doi.org/10.1038/ngeo1737, 2013.

Church, G., Bauder, A., Grab, M., Rabenstein, L., Singh, S., and Maurer, H.: Detecting and characterising an englacial conduit network within a temperate Swiss glacier using active seismic, ground penetrating radar and borehole analysis, Annals of Glaciology, 60, 193–205, https://doi.org/10.1017/aog.2019.19, 2019.

280 Church, G., Grab, M., Schmelzbach, C., Bauder, A., and Maurer, H.: Monitoring the seasonal changes of an englacial conduit network using repeated ground-penetrating radar measurements, The Cryosphere, 14, 3269–3286, https://doi.org/10.5194/tc-14-3269-2020, 2020.

Colorado, J., Devia, C., Perez, M., Mondragon, I., Mendez, D., and Parra, C.: Low-altitude autonomous drone navigation for landmine detection purposes, 2017 International Conference on Unmanned Aircraft Systems, ICUAS 2017, pp. 540–546, https://doi.org/10.1109/ICUAS.2017.7991303, 2017.

285 Cook, S. J. and Swift, D. A.: Subglacial basins: Their origin and importance in glacial systems and landscapes, Earth-Science Reviews, 115, 332–372, https://doi.org/10.1016/j.earscirev.2012.09.009, 2012.

Cuffey, K. M. and Paterson, W. S. B.: The Physics of Glaciers, Fourth Edition, Academic Press, fourth edn., 2010.

Flowers, G. E. and Clarke, G. K. C.: Surface and bed topography of Trapridge Glacier, Yukon Territory, Canada: digital elevation models and derived hydraulic geometry, Journal of Glaciology, 45, 165–174, https://doi.org/10.1017/S0022143000003142, 1999.

290 Fountain, A. G. and Walder, J. S.: Water flow through temperate glaciers, Reviews of Geophysics, 36, 299–328, https://doi.org/10.1029/97RG03579, 1998.

Fountain, A. G., Jacobel, R. W., Schlichting, R., and Jansson, P.: Fractures as the main pathways of water flow in temperate glaciers, Nature, 433, 618–621, https://doi.org/10.1038/nature03296, 2005.

Gaffey, C. and Bhardwaj, A.: Applications of Unmanned Aerial Vehicles in Cryosphere: Latest Advances and Prospects, Remote Sensing,
295 12, 948, https://doi.org/10.3390/rs12060948, 2020.

GLAMOS: The Swiss Glaciers 2013/14 and 2014/15, Bauder, A. (ed.), Glaciological Report No. 135/136 of the Cryospheric Commission (EKK) of the Swiss Academy of Sciences (SCNAT) published by VAW / ETH Zürich, Tech. rep., https://doi.org/10.18752/glrep_135-136, 2017.

Grab, M., Bauder, A., Ammann, F., Langhammer, L., Hellmann, S., Church, G. J., Schmid, L., Rabenstein, L., and Maurer, H. R.: Ice volume
300   estimates of Swiss glaciers using helicopter-borne GPR an example from the Glacier de la Plaine Morte, in: 2018 17th International Conference on Ground Penetrating Radar (GPR), pp. 1–4, IEEE, https://doi.org/10.1109/ICGPR.2018.8441613, 2018.

Grasmueck, M., Weger, R., and Horstmeyer, H.: Full-resolution 3D GPR imaging, Geophysics, 70, 12JF–Z26, https://doi.org/10.1190/1.1852780, 2005.

Gudmundsson, G. H., Bassi, A., Vonmoos, M., Bauder, A., Fischer, U. H., and Funk, M.: High-resolution measurements of spa-
305   tial and temporal variations in surface velocities of Unteraargletscher, Bernese Alps, Switzerland, Annals of Glaciology, 31, 63–68, https://doi.org/10.3189/172756400781820156, 2000.

Gulley, J.: Structural control of englacial conduits in the temperate Matanuska Glacier, Alaska, USA, Journal of Glaciology, 55, 681–690, https://doi.org/10.3189/002214309789470860, 2009.

Gulley, J. D., Benn, D. I., Müller, D., and Luckman, A.: A cut-and-closure origin for englacial conduits in uncrevassed regions of polythermal
310   glaciers, Journal of Glaciology, 55, 66–80, https://doi.org/10.3189/002214309788608930, 2009.

Hansen, L. U., Piotrowski, J. A., Benn, D. I., and Sevestre, H.: A cross-validated three-dimensional model of an englacial and subglacial drainage system in a High-Arctic glacier, Journal of Glaciology, pp. 1–13, https://doi.org/10.1017/jog.2020.1, 2020.

Harper, J. T., Bradford, J. H., Humphrey, N. F., and Meierbachtol, T. W.: Vertical extension of the subglacial drainage system into basal crevasses, Nature, 467, 579–582, https://doi.org/10.1038/nature09398, 2010.

315 Hart, J. K., Rose, K. C., Clayton, A., and Martinez, K.: Englacial and subglacial water flow at Skálafellsjökull, Iceland derived from ground penetrating radar, in situ Glacsweb probe and borehole water level measurements, Earth Surface Processes and Landforms, 40, 2071–2083, https://doi.org/10.1002/esp.3783, 2015.

Hoffman, M. J., Andrews, L. C., Price, S. A., Catania, G. A., Neumann, T. A., Lüthi, M. P., Gulley, J., Ryser, C., Hawley, R. L., and Morriss, B.: Greenland subglacial drainage evolution regulated by weakly connected regions of the bed, Nature Communications, 7,
320   https://doi.org/10.1038/ncomms13903, 2016.

Hooke, R. L., Laumann, T., and Kohler, J.: Subglacial Water Pressures and the Shape of Subglacial Conduits, Journal of Glaciology, 36, 67–71, https://doi.org/10.3189/S0022143000005566, 1990.

Iken, A., Rothlisberger, H., Flotron, A., and Haeberli, W.: The uplift of Unteraargletscher at the beginning of the melt season - a consequence of water storage at the bed?, Journal of Glaciology, 29, 28–47, https://doi.org/10.1017/S0022143000005128, 1983.

325 Irvine-Fynn, T. D. L., Moorman, B. J., Williams, J. L. M., and Walter, F. S. A.: Seasonal changes in ground-penetrating radar signature observed at a polythermal glacier, Bylot Island, Canada, Earth Surface Processes and Landforms, 31, 892–909, https://doi.org/10.1002/esp.1299, 2006.

Irving, J. D. and Knight, R. J.: Removal of wavelet dispersion from ground-penetrating radar data, Geophysics, 68, 960–970, https://doi.org/10.1190/1.1581068, 2003.

330 Joughin, I., Das, S. B., King, M. A., Smith, B. E., and Howat, I. M.: Seasonal Speedup Along the Western Flank of the Greenland Ice Sheet, Science, 320, 781–783, https://doi.org/10.1126/science.1153288, 2008.

King, E. C.: The precision of radar-derived subglacial bed topography: A case study from Pine Island Glacier, Antarctica, Annals of Glaciology, 61, 154–161, https://doi.org/10.1017/aog.2020.33, 2020.

Lindner, F., Walter, F., Laske, G., and Gimbert, F.: Glaciohydraulic seismic tremors on an Alpine glacier, The Cryosphere, 14, 287–308,
335   https://doi.org/10.5194/tc-14-287-2020, 2019.

Lliboutry, L.: Physical Processes in Temperate Glaciers, Journal of Glaciology, 16, 151–158, https://doi.org/10.3189/S002214300003149X,
1976.

Lliboutry, L.: Local Friction Laws for Glaciers: A Critical Review and New Openings, Journal of Glaciology, 23, 67–95,
https://doi.org/10.3189/s0022143000029750, 1979.

340   Lliboutry, L.: Modifications to the Theory of Intraglacial Waterways for the Case of Subglacial Ones, Journal of Glaciology, 29, 216–226,
https://doi.org/10.3189/S0022143000008273, 1983.

Macgregor, K. R., Riihimaki, C. A., and Anderson, R. S.: Spatial and temporal evolution of rapid basal sliding on Bench Glacier, Alaska,
USA, Journal of Glaciology, 51, 49–63, https://doi.org/10.3189/172756505781829485, 2005.

Mair, D., Nienow, P., Sharp, M., Wohlleben, T., and Willis, I.: Influence of subglacial drainage system evolution on glacier surface motion:
345   Haut Glacier d'Arolla, Switzerland, Journal of Geophysical Research, 107, 2175, https://doi.org/10.1029/2001JB000514, 2002.

McClymont, A. F., Green, A. G., Streich, R., Horstmeyer, H., Tronicke, J., Nobes, D. C., Pettinga, J., Campbell, J., and Langridge, R.: Visu-
alization of active faults using geometric attributes of 3D GPR data: An example from the Alpine Fault Zone, New Zealand, Geophysics,
73, https://doi.org/10.1190/1.2825408, 2008.

Moorman, B. J. and Michel, F. a.: Glacial hydrological system characterization using ground-penetrating radar, Hydrological Processes, 14,
350   2645–2667, https://doi.org/10.1002/1099-1085(20001030)14:15<2645::AID-HYP84>3.0.CO;2-2, 2000.

Nanni, U., Gimbert, F., Vincent, C., Gräff, D., Walter, F., Piard, L., and Moreau, L.: Quantification of seasonal and diurnal dynamics of
subglacial channels using seismic observations on an Alpine glacier, The Cryosphere, 14, 1475–1496, https://doi.org/10.5194/tc-14-1475-
2020, 2020.

Nienow, P., Sharp, M., and Willis, I.: Temporal Switching Between Englacial and Subglacial Drainage Pathways: Dye Tracer
355   Evidence from the Haut Glacier D'arolla, Switzerland, Geografiska Annaler: Series A, Physical Geography, 78, 51–60,
https://doi.org/10.1080/04353676.1996.11880451, 1996.

Nienow, P., Sharp, M., and Willis, I.: Seasonal changes in the morphology of the subglacial drainage system, Haut Glacier d'Arolla,
Switzerland, Earth Surface Processes and Landforms, 23, 825–843, https://doi.org/10.1002/(SICI)1096-9837(199809)23:9<825::AID-
ESP893>3.0.CO;2-2, 1998.

360   Nye, J.: Glacier sliding without cavitation in a linear viscous approximation, 315, 381–403, https://doi.org/10.1098/rspa.1970.0050, 1970.

Palmer, S. J., Dowdeswell, J. A., Christoffersen, P., Young, D. A., Blankenship, D. D., Greenbaum, J. S., Benham, T., Bam-
ber, J., and Siegert, M. J.: Greenland subglacial lakes detected by radar, Geophysical Research Letters, 40, 6154–6159,
https://doi.org/10.1002/2013GL058383, 2013.

Peters, L. E., Anandakrishnan, S., Holland, C. W., Horgan, H. J., Blankenship, D. D., and Voigt, D. E.: Seismic detection of a subglacial lake
365   near the South Pole, Antarctica, Geophysical Research Letters, 35, 1–5, https://doi.org/10.1029/2008GL035704, 2008.

Podolskiy, E. A. and Walter, F.: Cryoseismology, Reviews of Geophysics, pp. 708–758, https://doi.org/10.1002/2016RG000526, 2016.

Rada, C. and Schoof, C.: Channelized, distributed, and disconnected: Subglacial drainage under a valley glacier in the Yukon, The
Cryosphere, 12, 2609–2636, https://doi.org/10.5194/tc-12-2609-2018, 2018.

Reynolds, J. M.: An introduction to applied and environmental geophysics, John Wiley & Sons, 1997.

370   Ridley, J. K., Cudlip, W., and Laxon, S. W.: Identification of subglacial lakes using ERS-1 radar altimeter, Journal of Glaciology, 39, 625–634,
https://doi.org/10.1017/S002214300001652X, 1993.

Röthlisberger, H.: Water Pressure in Intra- and Subglacial Channels, Journal of Glaciology, 11, 177–203, https://doi.org/10.1017/S0022143000022188, 1972.

Schoof, C.: Ice-sheet acceleration driven by melt supply variability, Nature, 468, 803–806, https://doi.org/10.1038/nature09618, 2010.

375 Sheriff, R. E. and Geldart, L. P.: Exploration Seismology, Cambridge University Press, https://doi.org/10.1017/CBO9781139168359, 1995.

Shreve, R. L.: Movement of Water in Glaciers, Journal of Glaciology, 11, 205–214, https://doi.org/10.3189/S002214300002219X, 1972.

Siegert, M. J., Carter, S., Tabacco, I., Popov, S., and Blankenship, D. D.: A revised inventory of Antarctic subglacial lakes, Antarctic Science, 17, 453–460, https://doi.org/10.1017/S0954102005002889, 2005.

Sipos, D., Planinsic, P., and Gleich, D.: On drone ground penetrating radar for landmine detection, in: 2017 First International Conference
380 on Landmine: Detection, Clearance and Legislations (LDCL), pp. 1–4, IEEE, https://doi.org/10.1109/LDCL.2017.7976931, 2017.

Stuart, G., Murray, T., Gamble, N., Hayes, K., and Hodson, A.: Characterization of englacial channels by ground-penetrating radar: An example from austre Brøggerbreen, Svalbard, Journal of Geophysical Research, 108, https://doi.org/10.1029/2003JB002435, 2003.

Sugiyama, S. and Gudmundsson, G. H.: Short-term variations in glacier flow controlled by subglacial water pressure at Lauteraargletscher, Bernese Alps, Switzerland, Journal of Glaciology, 50, 353–362, https://doi.org/10.3189/172756504781829846, 2004.

385 Temminghoff, M., Benn, D. I., Gulley, J. D., and Sevestre, H.: Characterization of the englacial and subglacial drainage system in a high Arctic cold glacier by speleological mapping and ground-penetrating radar, Geografiska Annaler, Series A: Physical Geography, 101, 98–117, https://doi.org/10.1080/04353676.2018.1545120, 2019.

Tsutaki, S., Sugiyama, S., Nishimura, D., and Funk, M.: Acceleration and flotation of a glacier terminus during formation of a proglacial lake in Rhonegletscher, Switzerland, Journal of Glaciology, 59, 559–570, https://doi.org/10.3189/2013JoG12J107, 2013.

390 Tuckett, P. A., Ely, J. C., Sole, A. J., Livingstone, S. J., Davison, B. J., Melchior van Wessem, J., and Howard, J.: Rapid accelerations of Antarctic Peninsula outlet glaciers driven by surface melt, Nature Communications, 10, https://doi.org/10.1038/s41467-019-12039-2, 2019.

Wu, K., Rodriguez, G. A., Zajc, M., Jacquemin, E., Clément, M., De Coster, A., and Lambot, S.: A new drone-borne GPR for soil moisture mapping, Remote Sensing of Environment, 235, 111 456, https://doi.org/10.1016/j.rse.2019.111456, 2019.

395 Zechmann, J. M., Booth, A. D., Truffer, M., Gusmeroli, A., Amundson, J. M., and Larsen, C. F.: Active seismic studies in valley glacier settings: Strategies and limitations, Journal of Glaciology, 64, 796–810, https://doi.org/10.1017/jog.2018.69, 2018.

Zwally, H. J., Abdalati, W., Herring, T., Larson, K., Saba, J., and Steffen, K.: Surface melt-induced acceleration of Greenland ice-sheet flow, Science, 297, 218–222, https://doi.org/10.1126/science.1072708, 2002.